During the course of the work described here a new effect was discovered which interfered with measurements of single transmission for some time. The new effect, which causes large single transmission results when extremely good geometry prevails, is now known to be a small angle scattering (extending to about 1°) which exists for unmagnetized iron, but which disappears when the iron is magnetized. In other words, it is some kind of small angle, magnetic scattering which disappears when the domains (not grains in this case) disappear by alignment. For the present investigation the scattering was investigated sufficiently to insure that it did not affect the results. A much more complete investigation is of course now under way.

Some of the topics investigated in the course of these measurements are worthy of much more extensive effort and it is intended to pursue them further as time permits. At the present time the "double transmission" effect (use of polarizer and analyzer magnets) is being studied, as well as the depolarization of neutron beams by passage through magnetic fields and through thin sheets of unmagnetized iron.

It is a pleasure to acknowledge our indebtedness to the many persons who have been of assistance during these experiments. Professors Bloch, Fermi, Halpern, Sachs, Teller, and Wick have contributed many invaluable discussions. Mr. T. Brill is responsible for the design and construction of all the electronic equipment we have used. Mr. H. Paine and Dr. J. A. Berger have helped greatly in the preparation and metallographic study of specimens. The cross-section curve for iron was obtained with the assistance of Mr. G. Arnold, and Mr. M. Burgy has aided in the later stages of the work.

PHYSICAL REVIEW VOLUME 73, NUMBER 11 JUNE 1, 1948

# Proton-Proton Scattering at 7 Mev*

I. H. DEARNLEY,** C. L. OXLEY, AND J. E. PERRY, JR.***
*Department of Physics, University of Rochester, Rochester, New York*

(Received February 27, 1948)

Scattering experiments have been performed with protons from the cyclotron scattered in hydrogen gas. Photographic plates were used in a camera which recorded simultaneously individual protons scattered at angles from 10.5° to 45°. 5000 tracks were counted in each of nine narrow angular ranges to give good statistical accuracy. An experimentally determined correction was necessary due to proton penetration of the edges of the slits which admitted scattered protons to the photographic plates. The energy of the protons was determined by magnetic deflection and from ionization ranges. Analysis of the results shows an $s$ phase shift somewhat lower than that predicted by extrapolation of the earlier low energy data as analyzed in terms of square well, Gauss, and meson potentials. On the assumption of central $p$ wave scattering the results are fitted by a $p$ phase shift of $-0.22°$ which corresponds to scattering from a repulsive square well with interior Coulomb potential, range $e^2/mc^2$ and height 2.2 Mev. Extending the Rarita-Schwinger neutron-proton interactions to the proton-proton system for a prediction of tensor ${}^3P$ wave scattering, we find that the experimental results are reconcilable with the "symmetrical" theory and with the "charged" theory as formally constructed by them. The "neutral" theory gives ${}^3P$ scattering in definite disagreement with the experimental results.

## I. INTRODUCTION

EXPERIMENTS on the anomalous scattering of protons by protons have been reported in the energy range from 200 to 2400 kev[1–3] with results consistent with nuclear distortion of Mott

* Parts of this work were presented by each author in partial fulfillment of the requirements for the Ph.D. at the University of Rochester.

** Now at General Electric Research Laboratory, Schenectady, New York.

*** Now at California Institute of Technology, Pasadena, California.

[1] N. P. Heydenburg, L. R. Hafstad, and M. A. Tuve, Phys. Rev. 56, 1048 (1939).

[2] Herb, Kerst, Parkinson, and Plain, Phys. Rev. 55, 998 (1939).

[3] G. L. Ragan, W. R. Kanne, and R. F. Taschek, Phys. Rev. 60, 628 (1941).

scattering in the $s$ wave alone.[4] Experiments at 7 Mev should yield information concerning the $^3P$ state in addition to providing further information concerning the $^1S$ state. Wilson and co-workers[5] have recently reported on scattering experiments at 8, 10, and 14.5 Mev. Their results give some indication of repulsive $p$ wave effects. The present experiments, which yielded results in substantial agreement with Wilson's, were carried out at a lower energy and by a completely different method.

## II. APPARATUS

The photograph of Fig. 1 shows the scattering apparatus in place at the cyclotron. The proton beam was collimated and its energy spread limited[6] by three circular beam defining holes which were 2 mm in diameter and were located as marked in Fig. 1. The first hole located at the cyclotron exit port was covered with aluminum foil to separate the gas atmospheres of the cyclotron and the scattering apparatus. Because of the remaining fringing field, the last beam-defining hole, located at the chamber entry, was offset from the chamber axis so that the beam travel through the part of the chamber effective for scattering recorded protons was closely axial. Because of the fringing field, the beam assumed an elliptical cross section after passing through the last defining hole. In the chamber the collimated beam showed a maximum half-angle spread of 0.36° in the horizontal and 0.17° in the vertical plane. Magnetic effects on the scattered protons were small and were calculated to have negligible effects on the determination of the differential cross sections.

With beam-defining holes aligned for maximum visually observed beam at the last defining hole, a beam current of about $3\times10^{-9}$ ampere entered the scattering chamber. During all experimental operations the cyclotron magnet current was adjusted so that the beam current to the brass surrounding the second beam defining hole was a maximum.

At the left of the chamber, as shown in Fig. 1, a removable back plate held vacuum and gas leads and the Faraday cage. This back plate was replaced by one bearing a glass window in order to align visually for axial travel of the beam through the scattering chamber.

Figure 2 shows a schematic view of the scattering chamber. The beam entered the chamber through the last of the three beam-defining holes and proceeded through the hydrogen, which filled the chamber, into the Faraday cage. Protons scattered by hydrogen passed through the small rectangular "scattering slits" above and below the main beam and entered the photographic plates, as indicated by Fig. 2. The position at which the proton entered the plate determined the angle at which it had been scattered. In the direction perpendicular to the plane of Fig. 2 scattered protons were limited to the central portion of the photographic plates by the slits.

Not shown in Fig. 2 are two plate holders, one above and one below the beam. They were designed to take 1-in.$\times$3-in. photographic plates and to position them accurately with respect to the scattering slits. To define "swath" areas in the photographic plates for track counting, the

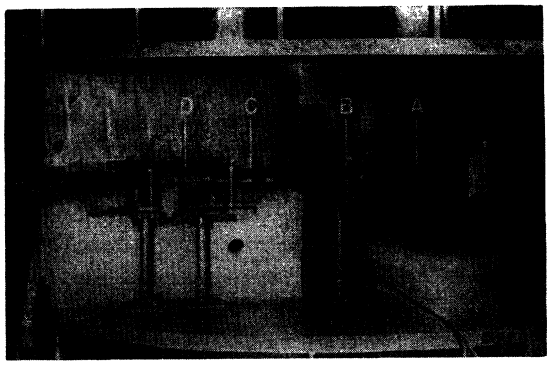


FIG. 1. Scattering apparatus at cyclotron. $A$, $B$, and $C$ show the locations of the beam defining holes, respectively, at the cyclotron exit port, in the flexible beam tube, and at the entry to the scattering chamber. The glass sections in the beam tube near the defining holes allowed for observation of the beam on fluorescent materials surrounding the holes, thus simplifying the adjustment of hole position. $D$ indicates the scattering chamber proper which is shown in schematic cross section in Fig. 2. The adjustable mounts for the chamber and beam tube are shown, as is part of the paraffin shield used around the chamber.

[4] G. Breit, H. M. Thaxton, and L. Eisenbud, Phys. Rev. 55, 1018 (1939).
[5] R. R. Wilson and E. C. Creutz, Phys. Rev. 71, 339 (1947); R. R. Wilson, Phys. Rev. 71, 384 (1947); Wilson, Lofgren, Richardson, Wright, and Shankland, Phys. Rev. 72, 1131 (1947).
[6] E. C. Creutz and R. R. Wilson, Rev. Sci. Inst. 17, 385 (1946).

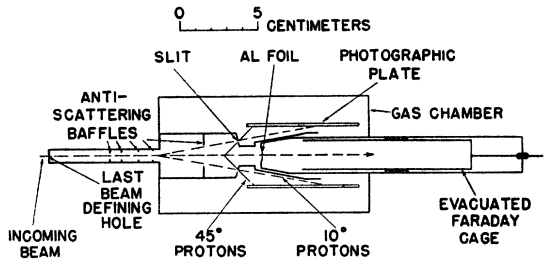


FIG. 2. Schematic drawing of scattering chamber in vertical cross section. All parts are of brass except as indicated and for the four small antiscattering baffles which are aluminum. The first antiscattering baffle at the left shielded the succeeding ones in the neck of the chamber from scattering by the edges of the last beam defining hole. The other neck baffles then prevented the useful part of the photographic plate from seeing any of the wall exposed to scattering from the edge of the first antiscattering baffle. The baffle in the large part of the chamber prevented protons from the last beam defining hole from striking the slits admitting scattered particles to the photographic plates.

plates were exposed before use to light through a grating ruled with lines every 0.25 mm. The lines were parallel to the one-inch edge of the plate. Exposure with an argon glow lamp made developable only the top grains of the emulsion so that during microscopic examination the proton tracks could be followed through these swath defining lines. Identical means of positioning the plates were used in the proton camera, the swath line camera, and the viewing microscope stage.

Difficulty was originally encountered with metallic scattering from baffles and chamber walls. The final baffle design, whose action is explained by the legend of Fig. 2, reduced metallic scattering to a very low level.

The details of the scattering slits are shown in Fig. 3. The plane of the slits was set at 10° to the vertical to favor the 10° scattering, since the number of protons per swath observed in our geometry is considerably higher for larger scattering angles. The form of the scattering slit edges constituted a special problem in the particular method used in these experiments. In conventional scattering experiments counters are normally used which record the scattering at any angle, after rotation to the correct angular position. The analyzer on the counter then has to accept scattering over only a small angular range. In the present experiments information at all angles from 10° to 45° was obtained simultaneously so the scattering slits were designed to present full aperture over this angular range. This accounts for the tapers of the slit jaws shown in Fig. 3. Such tapers had a very distinct disadvantage because they presented a penetrable area to protons. The extent of this area depended on their energy or scattering angle. In order to correct for this penetration, two additional rectangular slits were designed, one narrowed in the vertical direction and the other narrowed horizontally, as shown in Fig. 3. These were mounted at right angles to the "open slits" and were rotated into the active position before the plates for making the "closed slit" runs. Scattering experiments with both types of slits permitted calculation of the penetration effect.

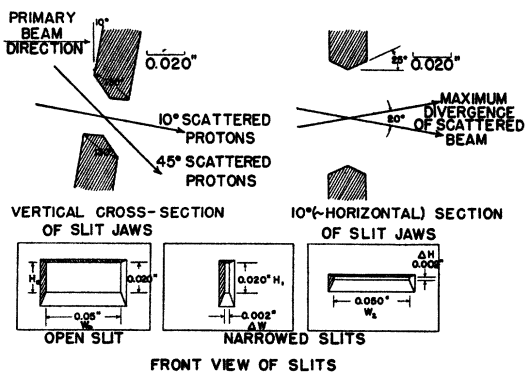


FIG. 3. Details of slits which admit scattered protons to the photographic plates. Dimensions shown are nominal.

The number of protons scattered through an angle $\Theta$ into a solid angle $\Delta\omega(\Theta)$ is given by the expression

$$N(\Theta)=\sigma(\Theta)n_i n_t 1(\Theta)\Delta\omega(\Theta), \qquad (1)$$

where $\sigma(\Theta)$ is the laboratory differential cross section per unit solid angle in units of cm$^2$, $n_t$ is the number of target hydrogen atoms per cm$^3$, $n_i$ is the number of incident protons in the beam, and $1(\Theta)$ is the effective target thickness or scattering length.

Under the assumption that hydrogen obeys the perfect gas law,[7] $n_t=1.4202\times10^{19}s\rho/T$ atoms/cc, where $s$ is the difference in height of the oil levels in the manometer used to measure the hydrogen pressure, $\rho$ is the density of the

[7] The numerical constants of these equations are derived with the values of the atomic constants given by R. T. Birge, Rev. Mod. Phys. 13, 233 (1941), and with the value $g=980.4$ cm/sec.$^2$ at Rochester.

manometer oil in grams per cm$^3$, and $T$ is the absolute temperature of the scattering gas. The number of incident protons is given by[7] $n_i = Q/e = 6.242 \times 10^{12} Q$, where $Q$ is the charge in microcoulombs collected during the run and $e$ is the proton charge in microcoulombs. Therefore[7]

$$N(\Theta) = 8.865 \times 10^{31} \sigma(\Theta) 1(\Theta) \Delta\omega(\Theta) R, \quad (2)$$

where $R = s\rho Q/T$ is called the run constant.

The scattering length is defined by a point on the photographic plate, and the height of the scattering slit as is shown in Fig. 4. In terms of the geometry of this figure the scattering length is calculated to be

$$1(\Theta) = hH \cos(\Theta - 10°)/ f\{1 - (H/2f)^2 \cos^2 10°\} \sin\Theta. \quad (3)$$

Since in the actual apparatus the plate holders were found to be not exactly parallel, $h$ and $f$ are functions of the scattering angle.

The solid angle effective for recorded protons in a swath and subtended at a scattering center of the beam is determined by the width, $W$, of the scattering slit and the swath width, $\Delta b$, on the plate. The solid angle geometry, assuming a beam with cross-section dimensions shrunk to form a line, is shown in Fig. 5. The solid angle for this case is given by

$$\Delta\omega(\Theta) = W\Delta b \sin^2(\Theta) \sin(\Theta - \delta\phi)/hg, \quad (4)$$

where again $h$ is a function of $\Theta$ and the plate is assumed inclined at an angle $\delta\phi$ with the horizontal.

The product $1(\Theta)\Delta\omega(\Theta)$, as defined above, must be corrected slightly in order to account for the finite dimensions of the beam, scattering slits, and swath width. These corrections are considered later.

The complete equation for the number of tracks per swath is then[7]

$$N(\Theta) = 8.865 \times 10^{31} \sigma(\Theta) R \times \frac{WH\Delta b \sin\Theta \cos(\Theta - 10°) \sin(\Theta - \delta\phi)}{gf\{1 - (H/2f)^2 \cos^2 10°\}}. \quad (5)$$

### III. DIMENSIONAL MEASUREMENTS

Most of the critical measurements were made by three independent observers with the aid of a Bausch and Lomb toolmakers' microscope and a Gaertner comparator. The instruments were checked against each other and against gauge blocks, errors apparently being less than 0.1 percent for nearly all distances measured.

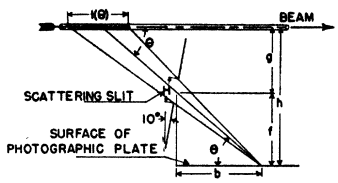


FIG. 4. Scattering length geometry.

The smallest distances, i.e., slit dimensions and swath width, could be measured directly, while the larger dimensions were found through a combination of two or more different measurements. Measurements were made at several places along the height and width of the slits. The swath width was measured on the swath line camera grating for those particular swaths counted in the final runs.

The vertical distance from the center of the beam to the center of a scattering slit was assumed to be the same for both upper and lower slits, since it was not possible to locate accurately the center of the beam. It can be shown that a slight vertical displacement in angle or position of the beam causes a negligible error in cross section, provided the cross section is computed from both upper and lower plates. Actually the cross section derived from the upper plates differed only slightly from that of the lower plates, so that the beam displacements were indeed small.

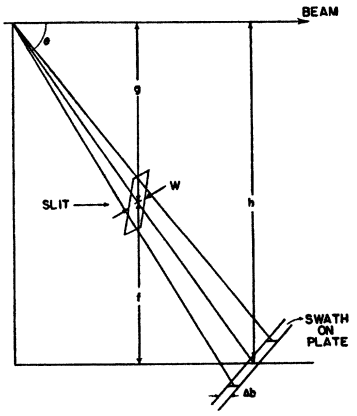


FIG. 5. Solid angle geometry.

TABLE I. Estimated uncertainty in dimensions.

| Dimension | Nominal length | Uncertainty | Percent uncertainty | Percent uncertainty in cross section at 20° |
|---|---|---|---|---|
| $\Delta b$ (10.5° to 20°) | 250$\mu$ | 0.5$\mu$ | 0.2 | 0.2 |
| $\Delta b$ (25° to 45°) | 250$\mu$ | 0.75$\mu$ | 0.3 | |
| $H$ (individual value) | 20 mil | 0.08 mil | 0.4 | 0.3 |
| $W$ (individual value) | 49 mil | 0.05 mil | 0.1 | 0.07 |
| $\Delta H$ | 2.05 mil | 0.05 mil | 2.5 | 0.3 |
| $\Delta W$ | 2.12 mil | 0.05 mil | 2.5 | 0.13 |
| $b$ | 0.39" to 2.2" | 2.0 mil | 0.5 to 0.1 | 0.32 |
| $f$ | 0.392" | 0.8 mil | 0.2 | 0.14 |
| $g$ | 0.395" | 0.4 mil | 0.1 | 0.1 |

The slit plate angle was checked to be 10° $\pm$0.1°. $\delta\phi$ was found from measurements of the slight warp of the plate holders.

Individual uncertainties estimated from the checks of the instruments and the consistency of independent measurements are given in Table I.

Uncertainties in scattering angle computed from errors in $b$ and $f$, amounted to $\pm$0.15° at 45° decreasing to $\pm$0.02° at 10.5°. The total uncertainty in cross section from all geometrical factors is about $\pm$0.7 percent for all angles. The extent to which this error is increased by the correction for slit jaw penetration is discussed later.

## IV. HYDROGEN SUPPLY AND PRESSURE MEASUREMENTS

Hydrogen was admitted to the scattering chamber through heated palladium tubes and was exhausted through a needle valve. With fixed hydrogen reservoir pressure and fixed heating current, the exhaust valve could be set to establish a practically constant hydrogen pressure of about 1.1-cm Hg in the scattering system. This pressure was chosen after calculations (following Breit, Thaxton, and Eisenbud[4]) showed multiple scattering would cause completely negligible effects.

The pressure was measured by a manometer containing octoil. The density of the octoil was measured in the temperature range 16°C to 36°C and was found to be 0.9803$\pm$0.0006 g/cc at 25°C with a temperature coefficient of $-$0.00075 g/cc per °C. The manometer was constructed of $\frac{1}{2}$-in. i.d. tubing about 5 ft. long. To reduce the effects of outgassing of the manometer oil and possible small stopcock leakage during periods of use, the closed side was provided with a 1-liter ballast flask. Oil levels were measured with a cathetometer.

## V. VACUUM SYSTEM

The vacuum system consisted of two branches exhausted by the same diffusion pump. One branch led to the Faraday cage, while the other evacuated the scattering chamber through a large "main" valve. There were two traps cooled with dry ice and acetone, one in the forepump line leading to the hydrogen exhaust valve, and one in the main pumping lead to the scattering chamber. Typical vacuums were $3\times10^{-5}$ mm Hg in the whole system with photographic plates present, $1.2\times10^{-5}$ mm Hg with no plates, and $5\times10^{-6}$ mm Hg in the Faraday cage with the main valve closed.

## VI. EXPERIMENTAL PROCEDURE

Hydrogen scattering runs were made in the following way. The camera was loaded with two plates and the system evacuated for about twelve hours, at which time the pressure was measured. No runs were started with a pressure greater than $4\times10^{-5}$ mm Hg. After thorough outgassing of the palladium tubes, the rate of rise of pressure in the scattering chamber was measured after closing the main valve. The cathetometer alignment was checked, the main valve closed, and the hydrogen flow started. During the next hour the charge measurement system was calibrated and the cyclotron turned on. From about 20 minutes before run time until the end of the run the manometer levels and the thermometers waxed to the manometer and scattering chamber were read at 5- or 10-minute intervals. At the end of the run the hydrogen flushing rate was measured. The scattering chamber was then put on the diffusion pump for about 30 minutes, during which time the charge apparatus calibration was repeated and final readings were taken to determine the small amount of manometer "leakage."

The hydrogen pressure varied smoothly during the hour-long runs, total variations being between $\frac{1}{2}$ mm and 5 mm (octoil) out of a total pressure of 16 cm of octoil. A constant rate of manometer leakage was assumed, and the consequent correction, amounting to at most 0.4

percent, was applied linearly with time. The sum of both manometer heights reflected very closely the change in manometer temperature, and indicated that the oil temperature was known to $\pm 0.3$°C. Uncertainties in the manometer readings, cathetometer scale, oil temperature, and scattering chamber temperature combine to give an error of $\pm 0.2$ percent in the term $s\rho/T$.

The charge was collected in forty small measured amounts, $\Delta Q$, at recorded times throughout the run by the automatic current integrator to be described later. In computing the run constant, large scale plots of $s\rho/T$ *vs.* time were used. The value of $s\rho/T$ at the center of each charge interval was multiplied by the corrected charge $\Delta Q$ collected during that interval. The sum of these products, i.e., the run constant, is considered good to $\pm 0.7$ percent in view of errors of 0.2 percent in $s\rho/T$, 0.5 percent in $Q$, and 0.1 percent from imperfect synchronization of charge and pressure readings.

## VII. CONTAMINATION

An estimate of the amount of impurity gas present during the scattering runs was obtained from the relative magnitudes of the hydrogen flushing rate and the rate of rise of pressure in the closed-off evacuated system. The average flow of hydrogen during the final open-slit scattering runs was 0.51 liter/sec. at the pressure of 11.4-mm Hg. For the same runs the average evolution of foreign gas was $1.6\times 10^{-5}$ liter-mm Hg/sec. Under the assumption of constant evolution with either hydrogen or vacuum, the equilibrium pressure of "air" was $3.2\times 10^{-4}$ mm Hg.

Evidence from terminal vacuums with and without photographic plates in the chamber indicated that at least half of the foreign gas was water vapor from the plates. The remainder was probably water vapor from the walls of the chamber and air entering through minute leaks. It is believed that the presence of 1 cm of hydrogen would not increase the evolution of water vapor, and might decrease it somewhat, relative to the rate in vacuum.

A calculation assuming Rutherford scattering with $Z=7$ gives the ratio of impurity tracks to hydrogen tracks to be 0.6 percent at 10.5°. This ratio decreases rapidly as the scattering angle increases. The uncertainty in the composition of the gas and in the calibration of the ion gauge used for the rate of rise measurements makes this estimate somewhat uncertain. A correction for contamination was therefore not applied to the cross section, but the contamination was considered in estimating the accuracy of the cross section at low angles.

## VIII. CHARGE MEASUREMENT

The number of individual protons passing through the scattering chamber during a run was measured by collecting the charge of the unscattered beam in a Faraday cage, which was separated from the scattering chamber by a 1-mil aluminum foil and evacuated by the diffusion pump. The charge was stored on a special dry air condenser. When the condenser potential reached about twelve volts, an automaton discharged the condenser and recorded the collection of a unit of charge.

The location and dimensions of the Faraday cage are shown in Fig. 2. During the series of runs the maximum observed ion gauge pressure in the Faraday cage system was $6\times 10^{-6}$ mm Hg. Estimates of the ionization from the currents observed in a similar cage by Herb, Kerst, Parkinson, and Plain[2] indicate that ionization currents were at the most about 0.1 percent of the proton current.

The entrance to the Faraday cage was in a magnetic field of about 2000 gauss because of the fringing field of the cyclotron. Calculation of electron paths in the magnetic field and extrapolation of the measurements of Herb, Kerst, Parkinson, and Plain[2] with a similar Faraday cage indicated that the field present was several times that necessary to prevent electrons from the 1-mil entrance foil from reaching the cage in appreciable numbers and to prevent secondary electrons in the interior of the cage from escaping. Neutralization of the proton charge in the foil is presumably negligible at this energy.

The entrance to the Faraday cage ($\frac{15}{32}$-in. diameter) allowed ample clearance for the beam ($\frac{1}{8}$ in.$\times\frac{3}{16}$ in.) to enter the cage. After the apparatus had been aligned in the usual manner, the centering of the beam on the Faraday cage entrance was tested by observing the darkening caused by the proton beam on a microscope cover glass placed over the cage entrance foil.

The Faraday cage was connected by a fifty-foot length of coaxial cable (capacitance about 0.002 $\mu$f) to the special air dielectric condenser in the cyclotron control room. The special condenser was required to overcome the soakage effects characteristic of mica condensers. The condenser and cable were found to have negligible soakage and leakage and to have a capacitance of about 0.021 $\mu$f. The potential of the condenser was measured with a Cenco-Dershman electrometer whose fixed quadrant voltages were supplied by small radio "B" batteries. The sharp light spot of the electrometer was arranged to pass through a slit to a photo-multiplier. When the condenser reached a potential of about twelve volts, the amplified photo-cell response closed a double-pole relay which discharged the condenser and made a chronograph record of the collection of a measured amount of charge. The discharge of the condenser passed through a ballistic galvanometer providing a convenient measure of charge for checking the performance of the automatic current integrator. During each scattering run a total of 40 condenser charges or about ten microcoulombs was collected.

The amount of charge required to trip the circuit was found to be closely constant over a series of chargings from an artificial source. (The average deviation from the mean charge was found to be 0.15 percent when observed by noting the ballistic galvanometer deflection for twenty five discharges.) The amount of charge necessary to trip the integrator was determined before and after each scattering run by measuring the time needed for a known current to trip the integrator. This current was supplied by a 500-volt regulated power supply through a high resistance and galvanometer. The galvanometer was calibrated in the normal fashion with a standard cell, recently certified by the Bureau of Standards, and laboratory standard resistors. Several weeks after the conclusion of the experiment this method of charge calibration as used was checked against a capacitance-potential measurement of the charge. The two methods agreed within about 0.15 percent.

A correction was found necessary because the electrometer spot lagged appreciably behind the condenser voltage, making the amount of charge necessary to trip the circuit dependent upon the rate of collection of charge. In actual operation the dependence of charge per integrator count upon charging rate was determined after each run by observing the ballistic galvanometer deflection for different charging rates. A correction to the calibration charge could then be made by comparing the rate of charging used for calibration with the rate of charging for each unit of charge collected during the run. This correction amounted to about 3 percent. The cyclotron conditions were sufficiently constant so that the time between discharges could be used in the correction to indicate the charging rate. Considering known random errors in measurement and correction, and the accuracy of the standards involved, the accuracy of the charge measurement is estimated to be about 0.5 percent.

## IX. DETECTION OF SCATTERED PROTONS

The use of the photographic plate as a detector in scattering experiments has been made practical by the development of improved fine grain emulsions which record a dense proton track against a low background of single developed grains even in the presence of considerable gamma-ray background. Although the counting of a large number of individual tracks is tedious, the method compares well with counter methods in convenience for the numbers of counts necessary to achieve an accuracy of one or two percent in the cross section. The observation of track length and direction provides high selectivity for the scattered protons against backgrounds of neutron recoils. The recording of all angles simultaneously makes changes in beam strength and hydrogen pressure affect all angles in the same way. Much data may be recorded on a few photographic plates, which are then available for subsequent re-examination.

The photographic plates used were Eastman Kodak alpha-particle plates with emulsions 25 microns thick. To prevent peeling of the emulsion in vacuum the edges of the plates were secured with cellulose tape. The plates exposed under the conditions of our experiments and processed according to the recommendations of the manufacturer showed easily identifiable proton tracks

and a low background of individual grains. The plates were dried slowly to minimize gelatin shifts. Any shift or contraction of the emulsion did not, however, effect the results, since plate positions and areas were fixed before proton exposure and processing by photographing the grid of swath lines in the emulsion.

After several preliminary runs which revealed correctable deficiencies in the apparatus, the following numbers of plates were exposed, as described, in the final runs:

(a) Four pairs of plates from four runs with the chamber evacuated and with the normal open slits.

(b) Four pairs of plates from runs with the hydrogen-filled chamber with normal open slits.

(c) Two pairs of plates from runs with a hydrogen-filled chamber but with one slit of each closed type.

(d) Two pairs of plates from runs as in (c) but with the positions of the slits before upper and lower plates reversed.

The proton tracks were observed by use of a binocular microscope at about 450× with dark field illumination supplied by a cardioid substage condenser. About 5000 tracks were counted for each of nine angles from 10.5 to 45 degrees. Because of the intensity distribution only one swath was counted at 45° on each plate, whereas at 10.5° five swaths were counted: increased resolution per swath at lower angles, however, maintained about the same angular resolution throughout the whole range of angles.

The tracks were counted by three observers, all swaths corresponding to a given angle being counted by one observer. Three weeks were consumed in the counting. The tracks counted were selected to eliminate tracks much shorter than the desired gas scattered proton tracks and those which proceeded in wrong directions. The individual observer's judgment sometimes determined whether a track should be eliminated. However, the criteria established for direction and length were such that no bona fide scattering track was eliminated and the correction procedure for spurious tracks should remove any effect of an observer's bias from the corrected results. Independent cross check counting by the three observers indicated that the ~5000 tracks at each angle could be counted to better than 0.5 percent. This uncertainty raises the statistical uncertainty in 5000 tracks from 1.4 to 1.5 percent.

## X. TREATMENT OF EXPERIMENTAL DATA

### Background Correction

At the pressures observed, the tracks found in the vacuum runs were due to scattering from metallic surfaces rather than from the residual gas in the chamber. In our calculations we assume that the number of these tracks is not changed appreciably by the presence of hydrogen in the chamber. This is reasonable, since these tracks originated largely from scattering by slit jaws and baffles, and with the design of the chamber used the small calculated beam spreading in hydrogen should effect this scattering little. The observed number of vacuum tracks was normalized to the charge of the open slit tracks and subtracted directly from the number of open slit tracks. This correction amounted to about 3 percent at 10.5 degrees and less than 1 percent at all other angles.

The closed slit runs were also corrected for vacuum scattering upon the assumption that the ratio of vacuum background tracks to total tracks is a constant independent of slit shape for a given angle. This seems to be justifiable, since the closed and open slits occupy closely the same position when in use and are therefore in the same spatial location relative to any sources of metallic scattering.

### Penetration Correction

We consider $N_0$, the number of open slit gas tracks per swath with the "vacuum" tracks subtracted out, to be composed of three components: protons that came through (a) the scattering slit opening, (b) the side slit jaws, and (c) the top and bottom slit jaws. The number of tracks per swath resulting from protons which came through the opening can be written as

$$N=\frac{WH\sin\Theta\cos(\Theta-10^\circ)\sin(\Theta-\delta\phi)}{gf[1-(H/2f)^2\cos^2 10^\circ]}$$

$$R_0\Delta b\sigma(\Theta)\times 8.865\times 10^{31}=K_0R_0\Delta b\alpha(\Theta), \quad (6)$$

where $R_0\Delta b$ is the run constant times the swath width averaged over the runs from which $N_0$ was obtained and

$$\alpha(\Theta)=\sigma(\Theta)\times 8.865\times 10^{31}. \quad (7)$$

The number of tracks caused by protons penetrating the side slit jaws is taken as proportional to the length of those jaws. This number of tracks per swath is given by

$$R_0\Delta b H_0\beta(\Theta), \tag{8}$$

where $H_0$ is the slit height and where $\beta(\Theta)$ is some function to be determined. The number of tracks caused by the protons passing through the top and bottom jaws of the scattering slit is taken proportional to the slit width $W_0$ and is given by

$$R_0\Delta b W_0\gamma(\Theta). \tag{9}$$

These expressions so far do not take into account penetration of the corners of the slits. On the assumption that the correction for the corners may be expressed as an increased effective width $\delta W$ and an increased effective height $\delta H$ of the slit, the equation for the total number of tracks per swath with open slits is

$$\frac{N_0}{R_0\Delta b}=\alpha K_0+\beta(H_0+\delta H)+\gamma(W_0+\delta W). \tag{10a}$$

Similar equations may be written for the narrow vertical slit (subscript 1) and narrow horizontal slit (subscript 2):

$$\frac{N_1}{R_1\Delta b}=\alpha K_1+\beta(H_1+\delta H)+\gamma(\Delta W+\delta W), \tag{10b}$$

$$\frac{N_2}{R_2\Delta b}=\alpha K_2+\beta(\Delta H+\delta H)+\gamma(W_2+\delta W), \tag{10c}$$

where the various symbols are defined in the same way as for the open slits.

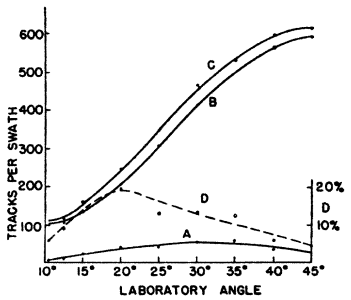


FIG. 6. Sources of tracks with open slits. *A* shows the number of tracks which penetrated the slit jaws, *B* shows the number of tracks which came through the slit opening proper, and *C* shows the total number of tracks being equal to the sum of the numbers shown by *A* and *B*. Curve *D* read with the scale at the right shows the ratio of penetration tracks to tracks from the slit opening.

The corner corrections, $\delta H$ and $\delta W$, whose effect on the cross section is at most 0.8 percent, were calculated as follows. The maximum amount of energy lost in the brass slit jaws by *counted* protons was computed from the lengths of the shortest tracks counted at each angle and the stopping power of the emulsion. The extent of the penetration region was then derived from the maximum path length in brass and the slit jaw angles. $\delta H$ and $\delta W$ were obtained from the area of the corners of the penetration region.

In the three simultaneous Eqs. (10) only the functions $\alpha$, $\beta$, and $\gamma$ are unknown. Solving simultaneously for them at each angle we obtained (a) the actual number of protons which have come through the slit opening and through the different slit jaws, and (b) the desired cross sections for proton-proton scattering. The distribution of proton tracks from various sources is shown in Fig. 6. From the first of the three equations one can determine what percentage of the total number of tracks are so-called penetration tracks. This ratio checks closely with that from a theoretical estimate of the translucent area of the slit jaws, which was made as in the corner corrections. This demonstrates that our method of taking care of the penetration effect for corner corrections is satisfactory.

The values of $\sigma(\Theta)$ derived from Eqs. (7) and (10) are given in column 2 of Table II for the corrected laboratory scattering angles. In columns 3 and 4 are the final laboratory and center of mass cross sections with certain small corrections described in the next section.

Table II lists two values for the 35-degree region, one for the average of both upper and lower plates, the other for the lower plates alone. These are listed because the cross section from the upper plates deviates a large amount (10 percent) from the smoothed cross-section curve. Physical causes for this deviation were sought in a re-examination of the upper plates. The deviation was largely due to one plate. The tracks were, however, dense and of good quality; there were no physical imperfections in the emulsion, no evidence of shadowing by superfluous material was found, and the number of tracks on the one plate were normal at other angles. The large deviation from the smoothed cross section (10 percent compared to a r.m.s. value of 1.9 per-

cent for all points) curve indicates that this point would possess undue influence in fitting the curve by least squares methods. In analysis of the data, we have preferred to make the calculations discarding the upper plates at thirty-five degrees, however, in the summary of the analysis values with the upper plate value at thirty-five degrees are included in parentheses.

## XI. SMALL CORRECTIONS

The scattered protons observed in any swath area on the photographic plate have been scattered through a range of angles about the nominal scattering angle at the center of the swath due to cross fire in the beam and to finite dimensions of the proton beam, slit, and swath. Because of the asymmetry of the distribution of angles in this small range the true average scattering angle differed from the nominal angle. The nominal angle was corrected by assuming an elliptical beam cross section of constant density and of extent determined from the size of the last defining hole and the visually observed dimensions of the beam spot at the rear of the scattering chamber. This assumption concerning the beam structure was born out by the observed track density across the swaths on the photographic plate. With this assumption the correction to the nominal angle was determined by averaging the angle over the finite dimensions and amounted to 2.3′ at 10° and 8.5′ at 45°. The corrected angles are given in Table II.

In addition to the change in average angle, the finite angular range and the second derivative of the cross section as a function of angle necessitated a small correction. This correction was calculated by finding the mean square angular deviation at the angles counted by use of the above assumptions concerning the beam structure, the cross fire in the beam estimated from its spreading, and the dimensions of the slit and swaths, and using the second derivative estimated from a theoretical $s$ wave cross section. This correction to the cross section varied from $-0.20$ percent at ten degrees to $+0.01$ percent at forty-five degrees.

The size of the beam, slits, and area in which tracks were counted on the photographic plates also make necessary corrections to the cross section calculated with the elementary considerations of geometry used thus far. A correction is necessary in the product of the "solid angle" and "scattering length" because of the finiteness of the dimensions noted. These corrections have been estimated by integrating over the dimensions of the slit and plate area and over the beam. The corresponding total correction to the cross section varies from $-0.46$ percent at 10.5° to $+0.33$ percent at 45°. This correction along with the one of the preceding paragraph has been included in the corrected cross sections of Table II.

TABLE II. Experimental proton-proton cross section at 7.03±0.06 Mev.

| Average lab. angle | Average lab. cross section | Corrected* lab. cross section | Center of mass cross section* |
|---|---|---|---|
| 10.51° | 40.56 $cm^2\times10^{-26}$ | 40.28 | 10.24 $cm^2\times10^{-26}$ |
| 12.59° | 29.38 | 29.21 | 7.48 |
| 15.06° | 25.48 | 25.36 | 6.56 |
| 19.95° | 23.29 | 23.21 | 6.17 |
| 24.99° | 23.03 | 22.98 | 6.34 |
| 30.00° | 22.60 | 22.56 | 6.51 |
| 34.83°** | 21.51** | 21.52** | 6.55** |
| 34.94°*** | 20.38*** | 20.40*** | 6.22*** |
| 39.87° | 20.34 | 20.38 | 6.64 |
| 44.62° | 18.75 | 18.81 | 6.61 |

* Corrected for small effects to be discussed in the next section.
** Lower plates only.
*** Lower and upper plates. See text for discussion of these two values.

## XII. ACCURACY OF RESULTS

The errors in most of the factors of Eq. (10) enter the cross section directly, unaltered by the correction for slit jaw penetration. On the other hand, the errors caused by slit dimensions and tracks counted are magnified considerably by the penetration correction process. Thus if there were no penetration, the error caused by counting 5000 tracks would be 1.5 percent, with an additional error of 0.3 percent from the slit dimensions. At 20°, for example, the correction process increases these errors to 2.5 percent and 0.5 percent, respectively. Similar magnification of these particular errors occurs at all angles, being largest at 20° where the penetration is relatively the greatest. The increase is of course due to the necessity of solving the simultaneous Eqs. (10) rather than the single Eq. (5).

The r.m.s. errors of all individual factors have been estimated. For convenience these are separated into two groups: the random errors of

individual points and "absolute" errors that affect the cross-section curve as a whole.

1. The total random error varies from ±2.2 percent at 10.5° to ±2.5 percent at 20° and down to ±2.1 percent at 45°. The sources are counting (about 2.3 percent) and uncertainty in scattering angle (about 0.25 percent).

2. The total "absolute" error is ±1.8 percent at 10.5 degrees and about ±1.4 percent for angles above 20°. The sources are (a) geometry, charge, pressure (1 percent for all angles), (b) hydrogen contamination (±0.6 percent at 10.5°, ±0.34 percent at 12.5°), and (c) effective uncertainty in cross section due to uncertainty in energy of incident protons (±1.4 percent at 10.5°, ±0.9 percent for 20° and above).

## XIII. MEASUREMENT OF PROTON ENERGY

The energy of the protons was determined from their range in air and their deflection in a magnetic field. In both types of experiments the beam was allowed to traverse the beam tube and scattering chamber in their normal positions, and, as in the scattering runs, the beam was monitored by maximizing the current to the second beam-defining hole.

### Range Experiments

Bragg curves of the protons in air were obtained by means of a "range" ionization chamber and a "monitor" ionization chamber, of the types described by Wilson.[8] Plots of the ratio of ionization currents (range/monitor) against the air distance to the center of the range ion chamber constituted the final Bragg curves. The observed air distance was corrected for the air temperature and pressure, for estimated effects of water vapor in the air, and for the Al foils at the scattering chamber and ionization chamber entry. The latter correction was measured by interposing, adjacent to the regular foils, two additional foils cut from the same sheets as the regular foils, and noting the consequent decrease in range.

The relationship between the extrapolated ionization range and the mean range is not known experimentally for protons of this energy. The necessary relationships were found by constructing Bragg curves by numerical integration of the specific ionizations of a single proton. The specific ionization of a single proton was taken to be proportional to the air atomic stopping cross section, as given by Livingston and Bethe[9] and modified at low energies in accordance with the revised Cornell Range-Energy Relation.[10] For these integrations we assumed Gaussian number-range distributions of the form

$$N(R)dR=\frac{dR}{(2\pi)^{\frac{1}{2}}\sigma_R}\exp\{-(R-R_M)^2/2\sigma_R^2\}. \quad (11)$$

Values of $\sigma_R=0.5$, 1.0, 1.5, and 2.0 cm were used.

The resulting relationships, of the type considered by Holloway and Livingston,[11] and Rado,[12] are

$$y=2.05\sigma_R, \quad (12a)$$

and

$$x=1.63\sigma_R-0.04, \quad (12b)$$

where $x$, $y$, and $\sigma_R$ are in cm and $0.5<\sigma_R<2.0$. The steep descent of the Bragg curve is extrapolated in both directions to intersect the range axis (at the extrap. ion. range) and a horizontal line through the maximum of the Bragg curve. $y$ is defined to be the range distance between these two intersections, while $x$ is the distance from mean range to extrapolated ionization range. Values of $x$ and $y$ are probably good to better than 10 percent. Other derived relations are (a) for a constant number of protons in a beam the maximum ordinate of a Bragg curve is proportional to $\sigma_R^{-0.424}$, and (b) the ratio of Bragg ordinate at the mean range to maximum Bragg ordinate is $0.775\pm0.005$ for $0.8<\sigma_R<2$ cm.

Bragg curves were taken after each of the four final open-slit hydrogen scattering runs, and after alternate narrow-slit runs. All curves gave the same extrapolated range within ±0.5 mm, but all showed the presence of two energy components in the beam. The relative intensity

[8] R. R. Wilson, Phys. Rev. 60, 749 (1941).

[9] M. S. Livingston and H. A. Bethe, Rev. Mod. Phys. 9, 245 (1937).

[10] Revised Cornell Range-Energy Relation, unpublished (1937).

[11] M. G. Holloway and M. S. Livingston, Phys. Rev. 54, 18 (1938).

[12] G. T. Rado, Thesis, Massachusetts Institute of Technology (1939).

and mean range of both components were found by subtracting two simple Bragg curves for the high energy component from our (average) compound Bragg curve. One of these was a theoretical curve with $\sigma_R = 1.27$ cm: the other, an experimental curve with, apparently, a very small amount of low energy component. (The latter curve was taken with a four-slit beam collimating system and with slightly different cyclotron conditions.) The compound, simple, and difference curves are shown in Fig. 7.

From these Bragg curves and the above theoretical relations the two energies were found to be $7.02 \pm 0.036$ Mev and $6.73 \pm 0.05$ Mev, with an intensity ratio of $8.4 \pm 1.4$. Uncertainty in the relative intensity arises from uncertainty as to which curve best represents the Bragg curve of the high energy component alone. The average from both subtraction processes is given above.

The average beam energy from the range experiments was $6.99 \pm 0.04$ Mev. This uncertainty includes the errors of temperature, pressure, and water vapor content of the air, position of the range ion chamber on the track, theoretical relations, air equivalence of Al foils, $\pm 30$ kv in the 1937 Cornell Range-Energy Relation, and the inaccuracy of the component intensity ratio.

### Magnetic Deflection Experiments

The auxiliary magnet used for the deflection experiments could not quite produce 90° focusing of 7-Mev protons. To measure the beam deflection a 4 in. $\times$ 10 in. spectrographic plate was placed in the field at a slight angle to the median plane of the gap. The beam through a narrow slit at the edge of the field hit this plate at nearly grazing incidence and left a curved trace of about 50° of arc. The radius of curvature was found from three points at the beginning, middle, and end of the trace, each point located transversely in the center of the trace. Energy and angular spreads in the high energy component made the trace rather broad even with a narrow slit, so that the three points could not be located very accurately.

The magnetic field was measured by means of a flip coil wound on a fused quartz form and calibrated at reduced fields by means of a proton nuclear induction experiment.[13] The values of $B = 13{,}480$ gauss and $\rho = 28.68 \pm 0.2$ cm yielded an energy of $7.11 \pm 0.1$ Mev for the high energy component of the beam. This is an average from five final plates exposed about two weeks after the final scattering runs. The size and unwieldiness of the magnet precluded making magnetic deflection and scattering runs concurrently. Range runs preceding and following the deflection runs showed no change in the beam since the scattering runs.

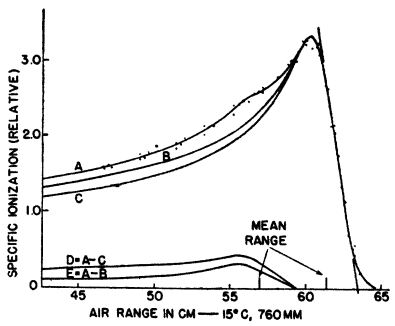


FIG. 7. Range ionization data. $A$ is the experimental curve for the conditions of the scattering experiments. It shows the presence of two energy components. $B$ is an experimental curve containing little low energy component. $C$ is the theoretical curve fitted to the high energy component. $D$ and $E$ are the residual ionization due to the low energy component after the high energy component, as represented by $B$ or $C$, respectively, is subtracted from $A$.

### Average Energy

The deflection experiments were considered less accurate than the range experiments and gave no usable information on the relative strengths of the beam components. Consequently, the final mean energy was calculated by averaging range and magnetic deflection values of the high energy and subtracting from this the 0.03 Mev found necessary in the range experiments to account for the low energy component. All energy experiments were done with fore vacuum in the beam tube and scattering chamber. When corrected for energy loss caused by hydrogen, the average beam energy at the scattering region was $7.03$ Mev $\pm 0.06$ Mev.

[13] F. Bloch, Phys. Rev. **70**, 460 (1946); F. Bloch, W. W. Hansen, and M. Packard, Phys. Rev. **70**, 474 (1946); W. R. Arnold and A. Roberts, Phys. Rev. **71**, 878 (1947).

## XIV. ANALYSIS OF RESULTS[14]

The theory of proton-proton scattering is well established. Formulas for the differential cross section in terms of the phase shift are given by Breit, Thaxton, and Eisenbud,[4] and Breit, Condon, and Present[15] who give references to other theoretical work. The treatment of scattering with tensor $^3P$ forces is given by Breit, Kittel, and Thaxton.[16]

### S Wave Analysis

The low energy proton-proton scattering experiments of Herb, Kerst, Parkinson, and Plain[2] and Heydenburg, Hafsted, and Tuve[1] in the range from 860 to 2400 kev were found by Breit, Thaxton, and Eisenbud[4] to be well represented by nuclear $s$ wave scattering from a square well of depth 10.5 Mev, radius $e^2/mc^2$. (Inclusion of Coulomb potential within the square well requires a depth of 11.3 Mev.) They were also fitted by a Gauss error well $A\exp(-\alpha r^2)$ with $A=51.44mc^2$ and $\alpha=21.59$ with a unit of length $9\times10^{-13}$ cm and with interior Coulomb potential. The experiments of Ragan, Kanne, and Taschek[3] in the range 200 to 300 kev were found to be in agreement with the $s$ wave scattering from the above square well. The phase shifts to be expected with these potentials at 7.03 Mev are given by Thaxton and Hoisington[17] as 53.8° for the square well and 54.0° for the Gauss error potential. The cross section for the square well is shown in Fig. 8 in comparison with the experimental results. It is seen that the experimental cross sections at higher scattering angles lie below the square well cross sections by about six percent.

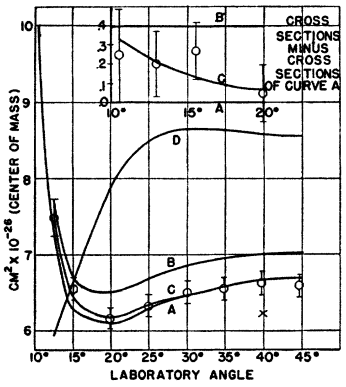


FIG. 8. Experimental 7-Mev differential cross sections in comparison with theory. The experimental points ⊼ show the estimated random uncertainty of each point. $X$ is the thirty-five degree value, including the upper plates (see text). A represents $s$ wave scattering alone as fitted to the experimental cross sections at high scattering angles. $B$ is the $s$ wave scattering expected from the 10.5 Mev, $e^2/mc^2$ square well which fits experiments in the range from 200 to 2400 kev. $C$ is fitted to the experimental points and includes $s$ and $p$ wave scattering on the basis of either central $p$ scattering or of "symmetrical" or "charged" tensor theories fitted by modification as described in the text. $D$ represents $B$ plus the $p$ wave scattering calculated from the Rarita-Schwinger "neutral" tensor interaction. The plot in the upper corner shows at low angles the differences of $B$, $C$, and experimental cross sections from the fitted $s$ wave curve, $A$. This plot best shows the experimental evidence for $p$ wave scattering.

Although central $p$ wave scattering is zero at forty-five degrees in the laboratory system, Breit, Kittel, and Thaxton[16] have shown that tensor $p$ wave scattering introduces an additional term in the cross section not zero at forty-five degrees. For small $p$ phase shifts, as may be expected, this term increases the cross section at forty-five degrees, so that presence of tensor $p$ wave scattering in addition to the square well scattering would increase the difference between our results and those predicted by extrapolating the low energy analysis with a square well. Assuming central $p$ wave scattering, the $s$ phase shift which best fits our results is $52.0°\pm0.6°$ ($51.6°\pm0.6°$).[18] This may be considered an upper limit to the actual $s$ phase shift since the presence of tensor $p$ wave scattering would require a smaller $s$ phase shift. Using the data of Thaxton and Hoisington,[17] we find that a square well with adjusted depth may be fitted to our experimental data and that at 1.4 Mev if the range of the square well is increased by $11\pm4$ percent. The accuracy of the $e^2/mc^2$ range assignment is given by Breit, Thaxton, and Eisenbud[4] as about 5 percent. The gauss error well would require similar adjustment in range to fit our experiments.

Hoisington, Share, and Breit[19] have also found

[14] One of us (C.L.O.) is responsible for the analysis.
[15] G. Breit, E. U. Condon, and R. D. Present, Phys. Rev. **50**, 825 (1936).
[16] G. Breit, C. Kittel, and H. M. Thaxton, Phys. Rev. **57**, 255 (1940).
[17] H. M. Thaxton and L. E. Hoisington, Phys. Rev. **56**, 1194 (1939).
[18] These values in parenthesis result from inclusion of the upper plate values at 35°.
[19] L. E. Hoisington, S. S. Share, and G. Breit, Phys. Rev. **56**, 884 (1939).

that the low energy scattering experiments may be fitted with a meson potential $Ce^{-r/a}\div r/a$ with $C=89.65mc^2$, $a=0.42e^2/mc^2$ and with interior Coulomb potential. Professor G. Breit and W. G. Bouricius have kindly calculated for us the phase shift expected with this potential. They find an $s$ phase shift 55.6 degrees, in even poorer agreement with our experimental phase shift than either the square well or gauss well values. This potential would require a larger increase in range to fit our experiments and a lowering of the meson mass from the value 326-electron masses which corresponds to this range.

The above discrepancy between our experiments and the extrapolated predictions with gauss error or square wells is not far outside the accuracies of the experiments and predictions. The discrepancy with the meson well is larger. Some of the apparent increase in range may be due to velocity dependence. More experiments which provide accurate absolute cross sections in this energy range would be valuable.

### Central $p$ Wave Analysis

The experimental results were analyzed by a least squares method for the $s$ and central $p$ phase shifts which best fit the data. The $p$ wave scattering observed is repulsive corresponding to a phase shift of $-0.22°\pm0.1°(0.28°\pm0.1°)$.[18] The fitted scattering with this phase shift is shown in Fig. 8, curve $C$, in comparison with the experimental cross sections. The r.m.s. deviation of the experimental points is 0.9 percent (1.9 percent)[18] from the fitted curve. The $p$ phase shift $-0.22°$ corresponds to a repulsive square well of range $e^2/mc^2$, height 2.2 Mev, and with interior Coulomb potential. This interaction is considerably weaker than the $^1S$ interaction which has a depth of 11.3 Mev[4] for the same range. The marked sensitivity of the $p$ phase shift to range has been noted in an exchange of letters by Peierls and Preston, and Foldy[20] in regard to the analysis of the experiments of Wilson *et al.*[5] Since tensor forces are probably present in the $^3P$ state, there is no need for further discussion of the central $p$ wave analysis here.

[20] R. E. Peierls and M. A. Preston, Phys. Rev. **72**, 250 (1947); L. L. Foldy, Phys. Rev. **72**, 731 (1947).

TABLE III. $^3P$ phase shifts for 7-Mev proton-proton scattering with Rarita-Schwinger interactions.

| Interaction | State $^3P_0$ | $^3P_1$ | $^3P_2$ |
|---|---|---|---|
| (I) "Symmetrical" | 1°16′ | −1°0′ | −19′ |
| (II) "Charged" | 7°57′ | −2°0′ | −50′ |
| (III) "Neutral" | −1°55′ | 14°53′ | 1°15′ |

### Calculation of Tensor $p$ Wave Scattering with the Rarita-Schwinger Interactions

Rarita and Schwinger[21] have constructed tensor neutron-proton interactions to agree with the observed quadrupole moment and binding energy of the deuteron and low energy neutron-proton scattering. For states of odd parity they have used three types of exchange relations suggested by meson theories and labeled (I) "Symmetrical," (II) "Charged," and (III) "Neutral." Their interactions are of square well type with range $e^2/mc^2$ as determined from the low energy proton-proton scattering experiments. It is of interest to adapt their interaction to the $^3P$ proton-proton scattering to indicate the nature of possible tensor effects.

The equality except for Coulomb interaction of neutron-proton and proton-proton interaction in like states is formally assumed. This equality has been found to hold closely in the $^1S$ state.[4] The neutron-proton interactions are then used with addition of the interior Coulomb potential to calculate the $^3P$ proton-proton scattering.[22] Of the three triplet states with $J=0$, 1, 2, $^3P_0$ and $^3P_1$ are not coupled to any other states, but $^3P_2$ is coupled to $^3F_2$. This coupling is small for the energy under consideration and is neglected in the calculation. The potentials as given by Rarita and Schwinger are for the "neutral" theory (III) $^3P_0$: 29.16 Mev, $^3P_1$: −35.41 Mev, $^3P_2$: −9.58 Mev. The potentials of the "charged"

[21] W. Rarita and J. Schwinger, Phys. Rev. **59**, 436 (1941); Phys. Rev. **59**, 550 (1941).

[22] The "symmetrical" potential is

$$V=\tfrac{1}{3}(\tau_1\cdot\tau_2)(\sigma_1\cdot\sigma_2)\{1-\tfrac{1}{2}g+\tfrac{1}{2}g\sigma_1\cdot\sigma_2+\gamma S_{12}\}J(r),$$

where $g$, $\gamma$, and the depth of the square well potential, $J(r)$, have been determined by Rarita and Schwinger from the neutron-proton system. The "charged" or "exchange" potential as formally assumed here may be written

$$V=\tfrac{1}{4}(1+\tau_1\cdot\tau_2)(1+\sigma_1\cdot\sigma_2)\{1-\tfrac{1}{2}g+\tfrac{1}{2}g\sigma_1\cdot\sigma_2+\gamma S_{12}\}J(r).$$

This potential is not to be confused with the potential given by the first-order charged meson theory which gives no force between like particles.

theory (II) have the same magnitude but are opposite in sign, and those of the "symmetrical" theory (I) are one-third those of the "charged" (II). The phase shifts were found using the series expansions of Yost, Wheeler, and Breit[23] for the interior regular Coulomb functions and their derivatives and for the exterior regular and irregular Coulomb functions and their derivatives. The values of the phase shifts given by Thaxton and Hoisington[17] for the 10.5 Mev, $e^2/mc^2$ attractive and repulsive square wells were checked with our values of the exterior functions. Values of the phase shifts for the $^3P$ states are given in Table III for 7-Mev scattering.

The differential cross sections for each of the theories is shown in Fig. 9 as calculated by the formula of Breit, Kittel, and Thaxton.[16] The $p$ wave scattering is added to the $s$ wave scattering from the 10.5 Mev, $e^2/mc^2$ square well. Shown in Fig. 10 are the $p$ wave effects in ratio to the $s$ wave scattering from the aforementioned square well. Also shown in Fig. 10 are the $p$ wave effects due to 10.5 Mev, $e^2/mc^2$ attractive and repulsive square wells as calculated by Eisenbud[24] from the phase shifts of Thaxton and Hoisington.[17] The theoretical $p$ wave effects are relatively most important near ten degrees at the end of the experimental range of angles.

The presence of the non-vanishing $p$ wave

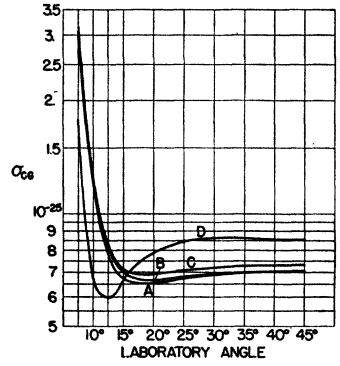


FIG. 9. Theoretical 7-Mev proton-proton scattering with Rarita-Schwinger tensor interactions. Shown is the differential cross section in cm² in the center of mass system. $A$ is $s$ wave scattering, due to the 10.5-Mev, $e^2/mc^2$ square well, to which the $p$ wave effects in $B$, $C$, and $D$ are added. $B$ includes $p$ wave scattering calculated with the "symmetrical" theory, $C$ with the "charged" theory, and $D$ with the "neutral" theory.

[23] F. L. Yost, J. A. Wheeler, and G. Breit, Phys. Rev. 49, 174 (1936).
[24] L. B. Eisenbud, private communication.

scattering at 45 degrees is peculiar to tensor force scattering. This term is negligibly small with the "symmetrical" theory, but appreciable with both "charged" and "neutral" theories. Scattering widely divergent from $s$ wave scattering, such as is predicted by the "neutral" theory, should be easily distinguishable.

The rather small difference between scattering with the "symmetrical" and "charged" theories may be understood from examination of the terms in the formula of Breit, Kittel, and Thaxton.[16] The cross-section expression contains three terms. The first contains the phase shifts as

$$\sum_{i=0}^{2} g_i \sin\delta_i \cos\delta_i,$$

where the $g_i$'s are the statistical weights and the $\delta_i$'s the phase shifts for the states $^3P_i$; the second term contains

$$\sum_{i=0}^{2} g_i \sin^2\delta_i,$$

and the third term, present only with tensor forces, depends on the differences of the phase shifts. The first term is the only appreciable one with central force scattering fitted to our experiments. It also predominates in the "symmetrical" theory, where the cancellation of effects of phase shifts of opposite signs leaves predominately repulsive scattering. The "symmetrical" scattering contains very little of the third or tensor term. In the charged theory, however, both second and third terms are appreciable and add,

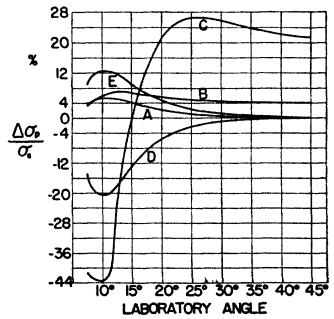


FIG. 10. Ratio at 7 Mev of theoretical nuclear $p$ wave scattering to $s$ wave scattering from a 10.5, $e^2/mc^2$ square well. $A$, $B$, and $C$ are calculated with the "symmetrical," "charged," and "neutral" tensor interactions of Rarita and Schwinger, respectively. $D$ and $E$ are due, respectively, to central $p$ wave scattering from attractive and repulsive 10.5-Mev, $e^2/mc^2$ square wells.

TABLE IV.

| Theory | $s$ phase shift | | Root mean square percent deviation of experiment from fitted curves |
|---|---|---|---|
| "Symmetrical" | 51.8°±0.6 | $c$ {0.60±0.3 | 0.8 |
| "Charged" | 50.8°±0.6 | $c$ {1.10±0.5 | 0.9 |
| Central | 52.0°±0.6 | Central phase shift: −0.22°±0.1 | 0.9 |
| If the value of cross section from the upper plates is included at 35 degrees the analysis becomes | | | |
| "Symmetrical" | 51.6° | $c$ {0.79 | 1.9 |
| "Charged" | 49.5° | $c$ {1.46 | 1.9 |
| Central | 51.6° | Central phase shift: −0.28° | 1.9 |

in the angular range under study, to give a constant addition to the center of mass cross section. The constant addition might also be closely represented by scattering caused by an increase in $s$ phase shift. The first term of the "charged" theory is smaller than in the "symmetrical" theory. The interactions, which are three times as intense in the "charged" theory, increase the attractive phase shifts more strongly to give a total first term still predominately repulsive but smaller in magnitude.

The symmetrical theory is then very similar in $^3P$ scattering to a central theory, and the "charged" scattering may be closely represented by central $p$ scattering plus a small amount of additional equivalent $s$ wave scattering. Thus if the actual scattering resembles either of these two theoretical predictions, it may not be possible to distinguish any tensor effects in the present experimental results.

Although the square well interactions must represent an oversimplification and the $^3P$ scattering may be sensitive to a change in well shape, it is not possible to estimate the $p$ wave effects with more reasonable well shapes without complete calculations. This is due to the cancellations of terms just noted.

## Comparison of Experimental Results with Tensor Theory Predictions

As shown by reference to Fig. 8, the experimental results are very decidedly in disagreement with the predictions of the "neutral" theory (curve $D$).

In order to test the agreement of the "symmetrical" and "charged" predictions with experiment, a least squares analysis was made to determine the $s$ phase shift and the fraction $c$ of the theoretical $p$ wave scattering which best fitted our results. The conclusions from this analysis are presented in Table IV with the results of the central analysis.

It will be noted that both the "symmetrical" and "charged" theories give reasonable agreement with experiment, as indicated by $c$ values close to 1. The "charged" theory, however, because of the tensor scattering term appreciable at forty-five degrees, requires a decrease of the $s$ phase shift which increases the discrepancy between the experimental $s$ phase shift and that predicted by extrapolation of the low energy experiments. (53.8° for square well, 54.0° for Gauss error, and 55.6° for meson.)

The combinations of the $p$ wave scattering of the "charged" and "symmetrical" theories, as modified by the $c$ factors with the scattering corresponding to the best $s$ phase shifts, differ at all angles by less than 0.2 percent from the fitted central scattering and are all shown by curve $C$ in Fig. 8. There is no indication for the need of tensor forces, but the strong tensor interaction of the "charged" theory causes wider disagreement with the extrapolated $s$ phase shift because of the appreciable "tensor" term in the scattering.

The determination of the amount of $p$ wave effect depends upon the relative values of the scattering at small angles to that at large angles. The sensitivity of the strength of the $p$ wave scattering to the absolute values of the cross section was indicated by analysis of the data with all experimental cross sections increased by 6 percent. This adjustment of the cross sections fitted the scattering at 45° to that expected from a 10.5-Mev, $e^2/mc^2$ square well. This analysis showed that an increase of approximately 50

percent in the strength of the $p$ wave scattering was required. The estimated experimental uncertainty in the over-all experimental curve is, however, estimated at less than two percent.

## XV. CONCLUSION

The photographic method has been shown to have certain advantages in proton-proton scattering experiments. As used here, the chief disadvantage is the need for a large correction for penetration of slit edges. Experiments by another group at Rochester are nearing completion. Their apparatus has been enlarged and slit construction modified so as to make the correction very small. The further experiments should provide a check of the reliability of our absolute cross sections and a check of the relative cross sections with a new geometry.

Analysis of the results has indicated a somewhat smaller $s$ phase shift than would be predicted from the extrapolation of the low energy data as analyzed with square well, Gauss, and meson potentials. This result depends upon the accuracy of our absolute cross sections at larger angles. This effect may be, of course, due in part to velocity dependence of the potentials, an effect which has not been considered here.

The $p$ wave analysis shows a small repulsive effect which may be fitted with central $p$ wave scattering but which also agrees with the $p$ wave scattering from the square well tensor interaction of Rarita and Schwinger labeled by its exchange properties as "symmetrical." The "charged" exchange of Rarita and Schwinger provides a less satisfactory fit when considered with the $s$ phase shift expected from low energy experiments. The "charged" theory also has no clear connection with actual meson theories.

Experiments at 7 Mev are not sensitive to the large difference in strengths of the $^3P$ interactions in the "symmetrical" and "charged" theories. As Ashkin and Wu[25] indicate in their analysis of proton scattering at 100 and 200 Mev, experiments in this energy range will be quite sensitive to the strengths of the triplet interactions.

## ACKNOWLEDGMENTS

We should like to acknowledge financial aid from the Research Corporation which, through a grant to Professor S. W. Barnes, supported this work in part. One of us (J. E. P.) was recipient during part of this work of a fellowship established by E. I. du Pont de Nemours and Company.

We gratefully acknowledge the continued interest and suggestions of Professor S. W. Barnes who suggested the problem to us and designed the early form of the apparatus. In addition, we received encouragement and help from Professors S. N. Van Voohris, R. E. Marshak, and Julius Ashkin. We also appreciate the aid of Mrs. Oxley who performed many of the numerical calculations. Many members of the laboratory and staff generously contributed suggestions, time, and equipment.

*Note Added in Proof:* Preliminary results of experiments by the second Rochester group indicate larger values of absolute cross sections than those given here.

[25] J. Ashkin and T. Y. Wu, Phys. Rev. **73**, 973 (1948)

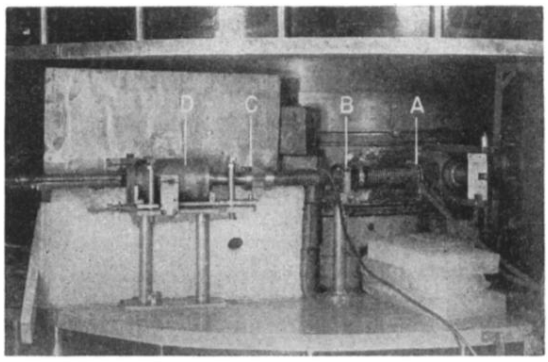


FIG. 1. Scattering apparatus at cyclotron. *A*, *B*, and *C* show the locations of the beam defining holes, respectively, at the cyclotron exit port, in the flexible beam tube, and at the entry to the scattering chamber. The glass sections in the beam tube near the defining holes allowed for observation of the beam on fluourescent materials surrounding the holes, thus simplifying the adjustment of hole position. *D* indicates the scattering chamber proper which is shown in schematic cross section in Fig. 2. The adjustable mounts for the chamber and beam tube are shown, as is part of the paraffin shield used around the chamber.